J. Fluid Mech. (2010), *vol.* 649, *pp.* 103–113.
doi:10.1017/S0022112009994071

Scaling of near-wall turbulence in pipe flow

MARCUS HULTMARK, SEAN C. C. BAILEY AND ALEXANDER J. SMITS†

Department of Mechanical and Aerospace Engineering, Princeton University, Princeton, NJ 08544, USA

(Received 20 May 2009; revised 16 December 2009; accepted 16 December 2009)

New measurements of the streamwise component of the turbulence intensity in a fully developed pipe flow at Reynolds numbers up to 145 000 indicate that the magnitude of the near-wall peak is invariant with Reynolds number in location and magnitude. The results agree with previous pipe flow data that have sufficient spatial resolution to avoid spatial filtering effects, but stand in contrast to similar results obtained in boundary layers, where the magnitude of the peak displays a prominent Reynolds number dependence, although its position is fixed at the same location as in pipe flow. This indicates that the interaction between the inner and outer regions is different in pipe flows and boundary layers.

1. Introduction

According to classical scaling arguments, the near-wall region in a turbulent wall-bounded flow scales with 'inner' variables, whereas the region away from the wall scales with 'outer' variables. The inner variables are the friction velocity $u_\tau = \sqrt{\tau_w/\rho}$, and the viscous length scale ν/u_τ, where τ_w is the shear stress at the wall, and ρ and ν are the fluid density and kinematic viscosity respectively. The outer region is assumed to have the same velocity scale as the inner region (u_τ), but the appropriate length scale is now the thickness of the shear layer, such as the pipe flow radius R, the boundary layer thickness δ or the half-channel height h.

Classical scaling works very well for the mean velocity profile, as comprehensively demonstrated by e.g. Zagarola & Smits (1998) and McKeon *et al.* (2004). It is not clear, however, that the turbulent stresses scale in this way, especially with regard to the streamwise component $\overline{u'^2}$. Here we focus on the region close to the wall where the distribution of $u^{+2} = \overline{u'^2}/u_\tau^2$ shows a distinct peak u^{+2}_{max} at $y^+ = yu_\tau/\nu \approx 15$. Mochizuki & Nieuwstadt (1996) concluded from a survey of data taken in boundary layer, pipe and channel flows that this peak is independent of Reynolds number, and therefore follows classical scaling. In contrast, boundary-layer data, including data from the high Reynolds number atmospheric surface layer, show that this peak increases significantly with Reynolds number (Fernholz *et al.* 1995; Marusic & Kunkel 2003). Some representative data are given in figure 1, along with the semi-empirical correlation suggested by Hutchins & Marusic (2007), which was based on the results of Marusic & Kunkel (2003):

$$u^{+2}_{max} = 1.036 + 0.965 \ln Re_\tau, \tag{1.1}$$

† Email address for correspondence: asmits@princeton.edu

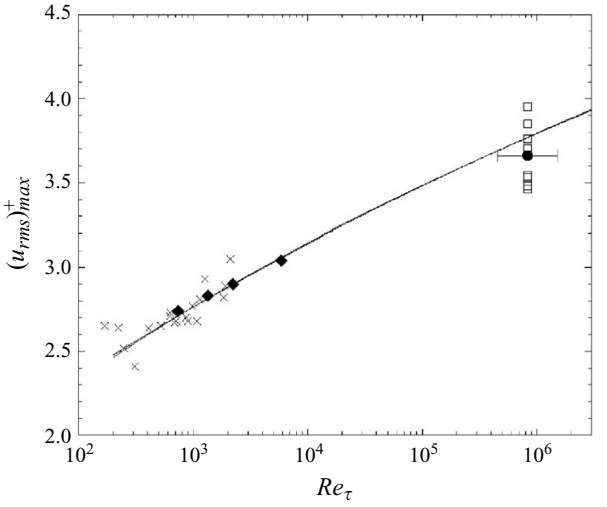

FIGURE 1. The magnitude of the near-wall peak in the streamwise turbulence intensity in turbulent boundary layers, as a function of Reynolds number. From Marusic & Kunkel (2003), where the original data sources are given.

where $Re_\tau = \delta u_\tau/\nu$. Marusic *et al.* (2010) suggest that this correlation for boundary layers may overestimate the rate at which the peak increases with Reynolds number. Hutchins *et al.* (2009) proposed that

$$u^{+2}_{max} = 4.837 + 1.075 \log_{10} Re_\tau. \tag{1.2}$$

Townsend (1961, 1976) and Bradshaw (1967) used this Reynolds number dependence of the peak to infer that the larger scales in the outer region of the boundary layer continue to affect the smaller scale motions in the inner region at all Reynolds numbers, and proposed the concepts of 'active' and 'inactive' motions to help explain the inner–outer interaction.

Our specific interest here is fully developed turbulent pipe flow. Results on the streamwise intensity from a number of previous studies are shown in figure 2. Although it is clear that there exists a peak in u^{+2} near $y^+ = 15$, the data display very significant scatter and it is difficult to draw any conclusions regarding Reynolds number scaling. Is the peak constant, or does it depend on Reynolds number? To try to settle this question, a new set of experiments was performed in fully developed pipe flow, with an emphasis on obtaining high accuracy data.

2. Experiments

Measurements of the streamwise component of the turbulence intensity were acquired for Reynolds numbers based on pipe diameter, Re_D, ranging from 24×10^3 to 145×10^3, where $Re_D = \langle U \rangle D/\nu$, $D = 2R$, and $\langle U \rangle$ denotes the area-averaged velocity. The experiments were conducted in the Princeton University/ONR Superpipe, described in detail by Zagarola (1996) and Zagarola & Smits (1998). Although this facility can be pressurized (it is the same facility used by Morrison *et al.* 2004, whose data are shown in figure 2), all experiments reported here were conducted at atmospheric pressure. The pipe was a commercial steel pipe with an average inner diameter of $D = 129.84$ mm and an overall length of $196D$. The friction velocity was found from the pressure drop along the pipe. The mean flow behaviour is described

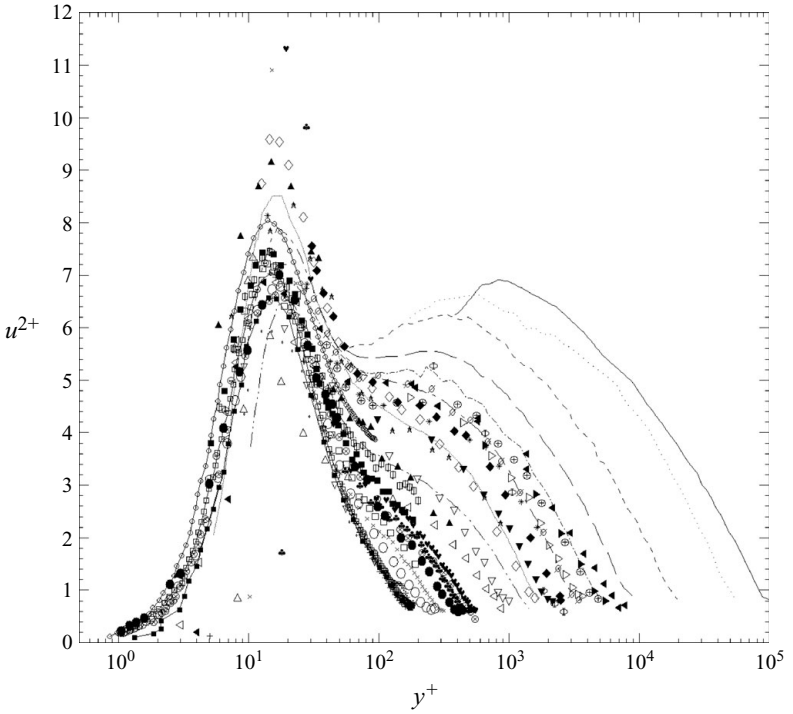

FIGURE 2. Streamwise turbulence intensity distributions for pipe flow plotted in inner coordinates. The data sources are given in table 1.

by Langelandsvik, Kunkel & Smits (2008), who showed that the pipe is hydraulically smooth for $Re_D < 8 \times 10^5$.

The experimental conditions and uncertainties are listed in tables 2 and 3, respectively. The best practices available were used in order to ensure the accuracy of the data. Single normal hot-wires with Wollaston wire (90 % Pt 10 % Rh) of diameter 2.5 μm and length between $l_w = 0.4$–1.8 mm were used for the measurements. A Dantec Streamware anemometer was used in the 1:1 bridge mode with an external resistor operated at an overheat ratio of 2.5 and measured frequency response above 60 kHz. The data were low-pass filtered at 30 kHz and digitized by a 16 bit A/D board (NI PCI-6123) at a rate of 60 kHz. The initial position of the wire y_0 was determined using a depth-measuring microscope (Titan Tool Supply, Inc.). The traverse was equipped with a linear encoder with 5 μm resolution. A rotary encoder was used in conjunction with the lead screw pitch to verify the output of the linear encoder. To calibrate the hot-wire, a Pitot probe was mounted on the traverse about 1.5 mm above the hot-wire, and the distance between the probes was measured using the depth-measuring microscope. The two probes were then positioned so that they were symmetrically placed on opposite sides of the pipe centreline. The mean velocity was found from the pressure difference between the Pitot probe and two static-taps in the pipe wall located at the same streamwise position. For all pressure measurements, it was found necessary to allow sufficient time for the pressure within the pressure tubing to reach a steady state and to use long averaging times to minimize the effects of transients on the average. For example, at the lowest velocities, 3 min were allowed between samples and data were sampled for 1 min. Pressure data were acquired using three separate transducers. Pitot pressures were acquired using a Datametrics 1400

Authors	Re_D	Medium	Method	l (mm)	l/d	l^+	Symbol
Eggels *et al.* (1994)	5.3×10^3	Air	HWA	1.0	200	4.0	○
Eggels *et al.* (1994)	5.45×10^3	Air	LDV	2.6	10.4	7.6	÷
Eggels *et al.* (1994)	5.45×10^3	Air	PIV	N/A	N/A	N/A	●
Eggels *et al.* (1994)	5.3×10^3	Air	DNS	N/A	N/A	N/A	-■-
Morrison *et al.* (2004)[a]	55×10^3	Air	HWA	0.5	200	11.6	-···-
Morrison *et al.* (2004)	75×10^3	Air	HWA	0.5	200	14.1	....
Morrison *et al.* (2004)	150×10^3	Air	HWA	0.5	200	25.9	− · −
Morrison *et al.* (2004)	230×10^3	Comp. air	HWA	0.5	200	39.4	-·-
Morrison *et al.* (2004)	410×10^3	Comp. air	HWA	0.25	100	33.1	—
Morrison *et al.* (2004)	1.0×10^6	Comp. air	HWA	0.25	100	76	- - -
Morrison *et al.* (2004)	3.1×10^6	Comp. air	HWA	0.25	100	213	. . .
Morrison *et al.* (2004)	5.7×10^6	Comp. air	HWA	0.25	100	385	—
Durst, Jovanovic & Sender (1995)[b]	7.4×10^3	Diesel oil	LDV	0.25	3.6	0.7	○
Durst *et al.* (1995)[b]	13.5×10^3	Diesel oil	LDV	0.25	3.6	1.1	●
Durst *et al.* (1995)[b]	20.8×10^3	Diesel oil	LDV	0.25	3.6	1.6	⊗
den Toonder & Nieuwstadt (1997)	4.9×10^3	Water	LDV	0.10	5	0.2	Θ
den Toonder & Nieuwstadt (1997)	10.0×10^3	Water	LDV	0.10	5	0.3	□
den Toonder & Nieuwstadt (1997)	17.8×10^3	Water	LDV	0.10	5	0.5	■
den Toonder & Nieuwstadt (1997)	24.6×10^3	Water	LDV	0.10	5	0.7	◫
Schildknecht, Miller & Meier (1979)[b,c]	17.25×10^3	Air	HWA	0.5	N/A	10	△
Morrison & Kronauer (1969)[d]	34×10^3	Air	HWA	1.0	N/A	13.6	▲
Morrison & Kronauer (1969)[d]	93×10^3	Air	HWA	1.0	N/A	33.4	⋆
Morrison & Kronauer (1969)[d]	193×10^3	Air	HWA	1.0	N/A	64.5	*
Lawn (1971)[d]	38×10^3	Air	HWA	1.0	N/A	13.9	▽
Lawn (1971)[d]	89×10^3	Air	HWA	1.0	N/A	29.7	▼
Lawn (1971)[d]	164×10^3	Air	HWA	1.0	N/A	51.5	▷
Lawn (1971)[d]	250×10^3	Air	HWA	1.0	N/A	75.3	▶
Laufer (1954)	46×10^3	Air	HWA	0.25	200	0.3	◁
Laufer (1954)	425×10^3	Air	HWA	0.25	200	1.9	◀
Perry & Abell (1975)	64×10^3	Air	HWA	1.35	338	39	◇
Perry & Abell (1975)	110×10^3	Air	HWA	1.35	338	63.4	◆
Perry & Abell (1975)	145×10^3	Air	HWA	1.35	338	80.6	⌀
Perry & Abell (1975)	215×10^3	Air	HWA	1.35	338	117	⊕
Sabot & Comte-Bellot (1976)[d]	135×10^3	Air	HWA	1.0	N/A	53	Φ
Grosse (2008)	5.0×10^3	Water	PIV	0.62	1	5.1	+
Grosse (2008)	10.1×10^3	Water	PIV	0.62	1	9.7	×
Grosse (2008)	17.7×10^3	Water	PIV	0.62	1	15.8	✤
Grosse (2008)	20.1×10^3	Water	PIV	0.62	1	17.7	♡
Wu & Moin (2008)	5.3×10^3	N/A	DNS	N/A	N/A	N/A	-○-
Wu & Moin (2008)	44×10^3	N/A	DNS	N/A	N/A	N/A	-□-

TABLE 1. Data sources for the streamwise turbulence intensity in pipe flow. Here, $Re_\tau = Ru_\tau/\nu$, l and d denote dimensions of the measurement volume, and $l^+ = lu_\tau/\nu$ uses the most relevant dimension of the measurement volume, and depends on the method.
[a]Re-examination of their lowest Reynolds number case has revealed insufficient calibration data at low velocities; [b]corrected for finite sensing volume; [c]suction holes may have affected results; [d]1 mm wire length assumed (length not reported). HWA, hot-wire anemometry; LDV, laser Doppler velocimetry; PIV, particle image velocimetry; DNS, direct numerical simulations.

Case	Re_D	Re_τ	$\langle U \rangle$ (m s^{-1})	l_w^+	y_0 (μm)
1	24 100	691	2.85	4.3	100
2	42 300	1137	4.96	7.0	80
3	78 500	1942	9.19	12.0	80
4	145 000	3336	17.0	20.6	100
5	23 800	689	2.82	19.1	60
6	40 800	1084	4.83	20.0	80
7	75 500	1867	8.93	19.4	115
8	23 700	692	2.80	12.8	70

TABLE 2. Experimental conditions.

Source	Uncertainty (±)
Pressure transducer	0.4 %
Temperature	0.1 %
Atmospheric pressure	0.2 %
Density (perfect gas law), ρ	0.3 %
Dynamic viscosity	0.4 %
Friction velocity, u_τ	0.8 %
Viscous length scale, ν/u_τ	0.9 %
Wall-normal position zero, y_0	10 μm
Wall-normal position accuracy, y	10 μm m^{-1}
Distance between Pitot and hot-wire	15 μm
Wall-normal distance in inner scaling, y^+	0.53 + 0.9 %
Calibration error due to calibration velocity	0.4 %
Calibration error due to probe positioning	0.005 %
Calibration error due to curve fitting	1.8 %
Mean velocity derived from hot-wire, U	2.2 %
Variance of velocity, $\overline{u'^2}$	3.0 %
Variance of velocity in inner scaling, u^{+2}	4.7 %

TABLE 3. Uncertainty estimates.

transducer with a 2488 Pa range, and corrected for viscous effects with the correlation proposed by Zagarola (1996). Streamwise pressure gradient data were acquired using an Omega PX653-0.05BD transducer with a 12.4 Pa range for the lower Reynolds numbers and a 133 Pa MKS Baratron transducer for the higher Reynolds numbers. Previous experiments and calibrations have shown excellent agreement between the Datametrics and Omega transducers at low pressures, verifying the linearity of the Datametrics transducer at low pressures. Twenty-eight calibration points were selected to cover the full range of profile measurements, with a bias towards the lower velocity range. The data were fitted using a fourth-order polynomial. Calibrations were performed before and after each velocity profile measurement and the agreement between both calibrations verified before data reduction. The flow temperature was kept constant to within ±0.2°C.

Table 3 shows that the main source of uncertainty in the measurements is the calibration of the hot-wire, due to uncertainties in measuring the calibration velocity and the accuracy of the curve fit. By necessity, the calibration range covered laminar and turbulent flow, and particular care was necessary to avoid positioning a major

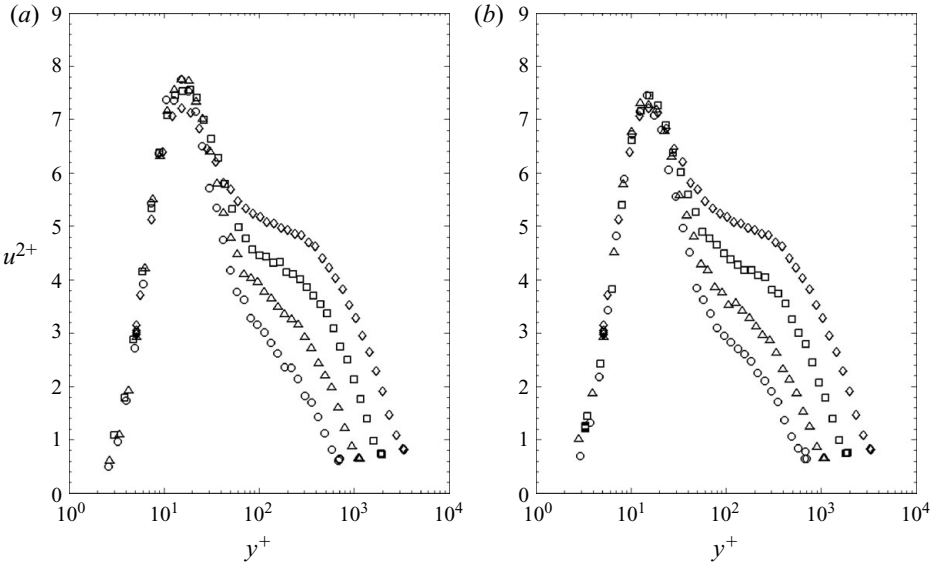

FIGURE 3. The streamwise turbulence intensities in inner coordinates (a) measured with constant wire length l_w and (b) measured with constant l_w^+ at ○, $Re_D = 24\,000$; △, $Re_D = 42\,000$; □, $Re_D = 78\,000$; ◇, $Re_D = 145\,000$.

part of the calibration range in the transitional flow regime. The error introduced by the curve fit decreased from ≈1.8 % at the lowest Reynolds number to ≈0.4 % at the highest Reynolds number. One important observation is that the error in the curve fit was higher close to the tails of the fit (up to twice as high), stressing the importance of calibrating over a range that is at least 10 % lower and higher in velocity than the extreme conditions expected during profile measurement.

A major difficulty in studies of turbulent wall-bounded flows is the limited spatial resolution of the probe (see, for example Ligrani & Bradshaw 1987*a*,*b*; Klewicki & Falco 1990; Hutchins *et al.* 2009; Chin *et al.* 2009). This problem is particularly evident at high Reynolds numbers where the size of the smallest eddies may be much smaller than the size of the probe, and this can lead to significant errors in the measurements of u^{+2}, especially in the near-wall region. Ligrani & Bradshaw (1987*a*) suggested that hot-wire probes will produce reliable statistics when the wire length, $l_w^+ \leqslant$ 20–25, where $l_w^+ = l_w u_\tau/\nu$. Hutchins *et al.* (2009) give a more quantitative description of the effects of spatial filtering and provide a correlation to help estimate the filtering effects as a function of Reynolds number and wire length. To investigate the effects of spatial filtering, two data sets were taken: one with a hot-wire of constant length $l_w = 0.4$ mm and another using wires with a constant value of $l_w^+ = 20 \pm 1$. At $Re_d = 25\,000$, additional measurements were taken using a wire with $l_w^+ = 12.8$.

3. Results and discussion

Figure 3(*a*) shows the distributions of u^{+2} acquired with the wire of constant length. The inner peak appears clearly at $y^+ \approx 15$. The three lower Reynolds numbers show a peak with constant magnitude of 7.68 ± 0.15. The uncertainty in the measurement is ± 0.37 at this location. The highest Reynolds number case has a slightly lower peak magnitude of 7.21, which may be due to spatial filtering.

Figure 3(*b*) shows profiles for the same Reynolds numbers acquired with wires of constant $l_w^+ = 20$. Here the magnitude of the peak is constant for all Reynolds numbers with a magnitude of 7.34 ± 0.13. The correlation given by Hutchins *et al.* (2009) to describe spatial filtering effects in a boundary layer includes the term l_w^+/Re_τ, implying that the filtering depends on Reynolds number, even at constant l_w^+. According to this correlation, the filtering effect at $Re_d = 150\,000$ with $l_w^+ = 20$ matches that at $Re_d = 25\,000$ with $l_w^+ = 12.8$. Comparing these two cases, we find that the magnitude of the peaks agreed to within 0.03, well within experimental error, and we conclude that spatial filtering is not masking any peak growth, although the true value for the peak magnitude is higher than that found with $l_w^+ = 20$. It is expected to be closer to the value found with $l_w^+ = 4$ which is 7.77 ± 0.37.

We now examine the previous pipe flow date more closely. In figure 4(*a*), the magnitude of u_{max}^{+2} determined simply by selecting the maximum value from figure 3(*b*) is compared with values extracted from figure 2, where only measurements with $l^+ < 25$ were selected to minimize the effects of spatial filtering. Despite the significant scatter, the magnitude of the peak shows no particular trend with Reynolds number. Especially interesting is the comparison with the data taken by den Toonder & Nieuwstadt (1997), which were acquired using laser Doppler anemometry with a spatial resolution of $l^+ < 0.7$ and a Reynolds number range that overlaps the current study. As shown separately in figure 4(*b*), the agreement in peak magnitude between the two data sets is remarkable, displaying a nearly constant value of about 7.3 from $167 < Re_\tau = Ru_\tau/\nu < 3336$. To compare this with the results from boundary layers, the correlations from Marusic & Kunkel (2003) and Hutchins *et al.* (2009) are also shown in figure 4(*b*) ((1.1) and (1.2), respectively), indicating a clear difference between pipe flows and boundary layers.

These results raise two interesting questions: why is there an apparent discrepancy between the near-wall scaling of pipe flows and boundary layers, and what will happen to the profiles of u^{+2} at very high Reynolds number?

To address the first question, we note that recent studies show that the outer-layer structure of internal and external flows displays some significant differences (Monty *et al.* 2007; Bailey *et al.* 2008), so the interaction between the inner and outer layers in these flows may well be different. Monty *et al.* (2009) and Mathis *et al.* (2009) further studied the differences at one specific Reynolds number $Re_\tau = 3000$ and found that there were significant differences in the spectra both in the inner and the outer regions. One possible explanation lies in the nature of the 'irrotational' contribution to the Reynolds stresses. Hinze (1975) shows that the contributions to the Reynolds shear stress in wall-bounded flows can be separated approximately into 'irrotational' and rotational components, where the irrotational component is loosely identified with the pressure fluctuations and the larger-scale motions of the outer region. The contribution from the irrotational component depends on the streamwise gradient of the difference between the normal stresses: for fully developed pipe flow it is zero, at least in the mean, while for zero-pressure-gradient boundary layers it is not.

To explore this first question further, we examine the energy-spectra for the velocity signal at the peak in u^{+2} using the local mean velocity to estimate the wavenumber. Figure 5 shows that the spectra in both inner and outer scaling. Here we see that even though the Reynolds stress scales on inner variables, neither inner nor outer scalings collapse the spectra over the entire Reynolds number range. In particular, although the spectra have some scatter, the outer scaled results do not show a strong collapse in the low wavenumber range, suggesting that the contribution to the energy from

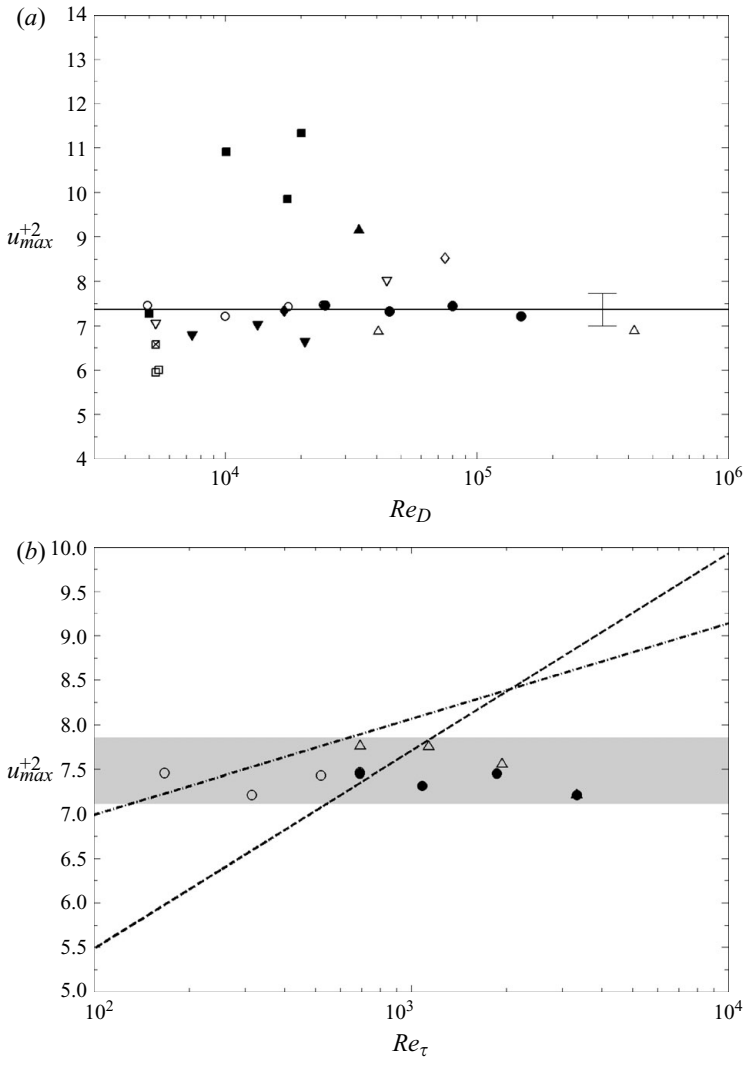

FIGURE 4. Magnitude of the near-wall peak in the streamwise turbulence intensity for pipe-flow studies with a spatial resolution better than $l^+ = 25$. (*a*) ●, present results obtained with $l_w^+ = 20$; ———, average value of present results, with corresponding error bar; ○, den Toonder & Nieuwstadt (1997); ▼, Durst *et al.* (1995); □, Eggels *et al.* (1994) (⊠= DNS); ■, Grosse (2008); △, Laufer (1954); ▲, Morrison & Kronauer (1969); ◇, Morrison *et al.* (2004); ◆, Schildknecht *et al.* (1979); ▽, Wu & Moin (2008) (DNS). (*b*) ●, present results obtained with $l_w^+ = 20$; △ present results obtained with $l_w = 0.4$ mm; ○, den Toonder & Nieuwstadt (1997). Dashed line is (1.1), and the dash-dotted line is (1.2). Shaded area corresponds to the estimated error for the present results.

these larger scales where the irrotational motions would be expected to contribute are not scaling over this Reynolds number range.

As to the second question, the results of Morrison *et al.* (2004) indicate that the magnitude of u^{+2} in the outer layer at their highest Re_D of 5.5×10^6 is still below the inner peak value measured in the current study. However, as shown in figure 3, turbulence in the outer layer continues to grow with Reynolds number while the inner peak remains constant. Unless the contribution to turbulent kinetic energy from

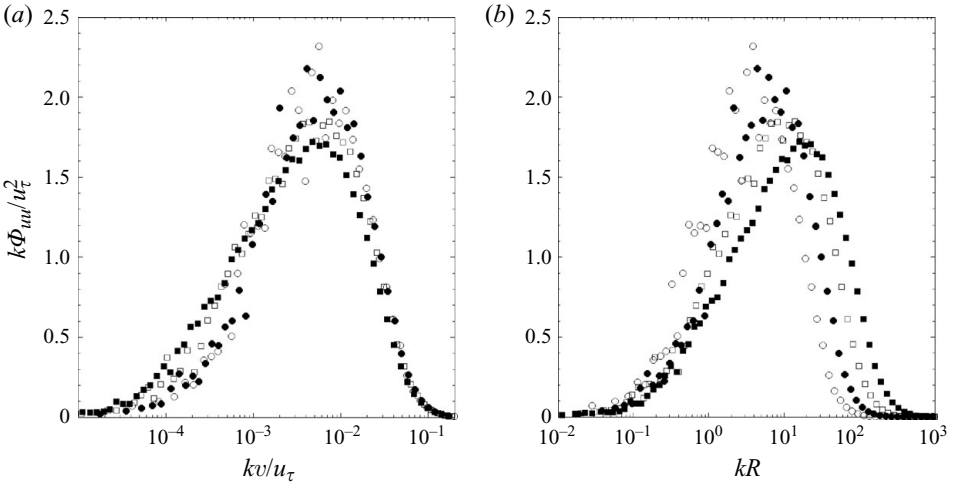

FIGURE 5. Pre-multiplied energy spectra of the streamwise velocity signal at the location of the inner peak for ○, $Re_D = 25\,000$; ●, $Re_D = 45\,000$; □, $Re_D = 80\,000$; ■, $Re_D = 145\,000$. Non-dimensionalized by (*a*) inner variables and (*b*) outer variables.

the smallest turbulence scales becomes negligibly small at high Reynolds number, the magnitude of u^{+2} in the outer layer will exceed that of the inner layer at some large Reynolds number. This suggests that at high Reynolds number there could be a fundamental change in the energy balance. For example, if the ratio of production to dissipation remains near unity in the overlap region, at high Reynolds number the rate of dissipation in this region will be higher than near the wall in the viscous layer.

4. Conclusions

Measurements of the streamwise component of the turbulence intensity were performed in a fully developed pipe flow with particular care taken to ensure accurate calibration at low velocities. The results indicate that the near-wall peak is invariant with Reynolds number in location and magnitude at Reynolds numbers up to 145 000 which compares well with other studies having sufficient spatial resolution to avoid spatial filtering effects. The invariance in the inner peak magnitude stands in contrast to similar results obtained in boundary layers, where a strong Reynolds number dependence has been observed.

This work was made possible by support received through NSF grant CTS-0625268, programme manager William Schultz and ONR grant N00014–09-1-0263, programme manager Ronald Joslin.

REFERENCES

BAILEY, S. C. C., HULTMARK, M., SMITS, A. J. & SCHULTZ, M. P. 2008 Azimuthal structure of turbulence in high Reynolds number pipe flow. *J. Fluid Mech.* **615**, 121–138.

BRADSHAW, P. 1967 Inactive motion and pressure fluctuations in turbulent boundary layers. *J. Fluid Mech.* **30**, 241–258.

CHIN, C. C., HUTCHINS, N., OOI, A. S. H. & MARUSIC, I. 2009 Use of direct numerical simulation (DNS) data to investigate spatial resolution issues in measurements of wall-bounded turbulence. *Meas. Sci. Technol.* **20** (11), 115401.

Durst, F., Jovanovic, J. & Sender, J. 1995 LDA measurements in the near-wall region of a turbulent pipe flow. *J. Fluid Mech.* **295**, 305–335.

Eggels, J. G. M., Unger, F., Weiss, M. H., Westerweel, J., Adrian, R. J., Friedrich, R. & Nieuwstadt, F. T. M. 1994 Fully developed turbulent pipe flow: a comparison between direct numerical simulation and experiment. *J. Fluid Mech.* **268**, 175–209.

Fernholz, H. H., Krause, E., Nockemann, M. & Schober, M. 1995 Comparative measurements in the canonical boundary layer at $Re_{\delta_2} \leqslant 6 \times 10^4$ on the wall of the German–Dutch windtunnel. *Phys. Fluids* **7** (6), 1275–1281.

Grosse, S. 2008 Development of the micro-pillar shear-stress sensor MPS3 for turbulent flows. PhD thesis, RWTH Aachen University.

Hinze, J. O. 1975 *Turbulence*, 2nd edn. McGraw Hill.

Hutchins, N. & Marusic, I. 2007 Evidence of very long meandering features in the logarithmic region of turbulent boundary layers. *J. Fluid Mech.* **579**, 1–28.

Hutchins, N., Nickels, T. B., Marusic, I. & Chong, M. S. 2009 Hot-wire spatial resolution issues in wall-bounded turbulence. *J. Fluid Mech.* **635**, 103–136.

Klewicki, J. C. & Falco, R. E. 1990 On accurately measuring statistics associated with small-scale structure in turbulent boundary layers using hot-wire probes. *J. Fluid Mech.* **219**, 119–142.

Langelandsvik, L. I., Kunkel, G. J. & Smits, A. J. 2008 Flow in a commercial steel pipe. *J. Fluid Mech.* **595**, 323–339.

Laufer, J. 1954 The structure of fully developed pipe flow. *Tech. Rep.* NACA 1174. National Advisory Committee for Aeronautics.

Lawn, C. J. 1971 The determination of the rate of dissipation in turbulent pipe flow. *J. Fluid Mech.* **48**, 477–505.

Ligrani, P. M. & Bradshaw, P. 1987*a* Spatial resolution and measurement of turbulence in the viscous sublayer using subminiature hot-wire probes. *Exper. Fluids* **5**, 407–417.

Ligrani, P. M. & Bradshaw, P. 1987*b* Subminiature hot-wire sensors: development and use. *J. Phys.* E*: Sci. Instrum.* **20**, 323–332.

Marusic, I. & Kunkel, G. J. 2003 Streamwise turbulence intensity formulation for flat-plate boundary layers. *Phys. Fluids* **15** (8), 2461–2464.

Marusic, I., McKeon, B. J., Monkewitz, P. A., Nagib, H. M., Smits, A. J. & Sreenivasan, K. R. 2010 Wall-bounded turbulent flows: recent advances and key issues. *J. Fluid Mech.* (in press).

Mathis, R., Monty, J. P., Hutchins, N. & Marusic, I. 2009 Comparison of large-scale amplitude modulation in turbulent boundary layers, pipes, and channel flows. *Phys. Fluids* **21** (11), 111703.

McKeon, B. J., Li, J., Jiang, W, Morrison, J. F. & Smits, A. J. 2004 Further observations on the mean velocity in fully developed pipe flow. *J. Fluid Mech.* **501**, 135–147.

Mochizuki, S. & Nieuwstadt, F. T. M. 1996 Reynolds-number-dependence of the maximum in the streamwise velocity fluctuations in wall turbulence. *Exper. Fluids* **21**, 218–226.

Monty, J. P., Hutchins, N., Ng, H. C. H., Marusic, I. & Chong, M. S. 2009 A comparison of turbulent pipe, channel and boundary layer flows. *J. Fluid Mech.* **632**, 431–442.

Monty, J. P, Stewart, J. A., Williams, R. C. & S., Chong M. 2007 Large-scale features in turbulent pipe and channel flows. *J. Fluid Mech.* **589**, 147–156.

Morrison, J. F., McKeon, B. J., Jiang, W. & Smits, A. J. 2004 Scaling of the streamwise velocity component in turbulent pipe flow. *J. Fluid Mech.* **508**, 99–131.

Morrison, W. R. B. & Kronauer, R. E. 1969 Structural similarity for fully developed turbulence in smooth tubes. *J. Fluid Mech.* **39**, 117–141.

Perry, A. E. & Abell, C. J. 1975 Scaling laws for pipe-flow turbulence. *J. Fluid Mech.* **67**, 257–271.

Sabot, J. & Comte-Bellot, G. 1976 Intermittency of coherent structures in the core region of fully developed turbulent pipe flow. *J. Fluid Mech.* **74**, 767–797.

Schildknecht, M., Miller, J. A. & Meier, G. E. A. 1979 The influence of suction on the structure of turbulence in fully developed pipe flow. *J. Fluid Mech.* **90**, 67–107.

den Toonder, J. M. J. & Nieuwstadt, F. T. M. 1997 Reynolds number effects in a turbulent pipe flow for low to moderate *Re*. *Phys. Fluids* **9** (11), 3398–3409.

Townsend, A. A. 1961 Equilibrium layers and wall turbulence. *J. Fluid Mech.* **11**, 97–120.

Townsend, A. A. 1976 *The Structure of Turbulent Shear Flow*. Cambridge University Press.

Wu, X. & Moin, P. 2008 A direct numerical simulation study on the mean velocity characteristics in turbulent pipe flow. *J. Fluid Mech.* **608**, 81–112.

Zagarola, M. V. & Smits, A. J. 1998 Mean-flow scaling of turbulent pipe flow. *J. Fluid Mech.* **373**, 33–79.

Zagarola, M. V. 1996 Mean-flow scaling of turbulent pipe flow. PhD thesis, Princeton University, Princeton.